Carbohydrate Polymers 322 (2023) 121286

Contents lists available at ScienceDirect

Carbohydrate Polymers

journal homepage: www.elsevier.com/locate/carbpol

Characterisation of locust bean gum with asymmetric flow field-flow fractionation (AF4) and light scattering

Adam O'Connell [a], Yadira González-Espinosa [b], Francisco M. Goycoolea [b], Peter Schuetz [c], Johan Mattsson [a,*]

[a] School of Physics and Astronomy, University of Leeds, Leeds LS2 9JT, United Kingdom
[b] School of Food Science and Nutrition, University of Leeds, Leeds LS2 9JT, United Kingdom
[c] Unilever R&D, Colworth, MK44 1LQ, United Kingdom

ARTICLE INFO

Keywords:
Locust bean gum
Galactomannans
AF4
MALS
Structure
Aggregation

ABSTRACT

We present a detailed characterisation of locust bean gum (LBG), an industrially significant galactomannan, utilising asymmetric flow field-flow fractionation (AF4) and light scattering. Molecular weight and size determination of galactomannans is complicated by their tendency to aggregate, even in dilute solutions; AF4 allows us to confirm the presence of aggregates, separate these from well-dispersed polymer, and characterise both fractions. For the dispersed polymer, we find $M_w = 9.2 \times 10^5$ g mol^{-1} and $R_{g,z} = 82.1$ nm; the distribution follows Flory scaling ($R_g \sim M^{\nu}$) with $\nu \sim 0.63$, indicating good solvent conditions. The aggregate fraction exhibited radii of up to 1000 nm and masses of up to 3×10^{10} g mol^{-1}. Furthermore, we demonstrate how both fractions are influenced by changes to filtration procedure and solvent conditions. Notably, a 200 nm nylon membrane effectively removes the aggregated fraction; we present a concentration-dependent investigation of solutions following this protocol, using static and dynamic light scattering, which reveals additional weak aggregation in these unfractionated samples. Overall, we demonstrate that AF4 is highly suited to LBG characterisation, providing structural information for both well-dispersed and aggregated fractions, and expect the methods employed to apply similarly to other galactomannans and associating polymer systems.

1. Introduction

Galactomannans are a class of naturally occurring polysaccharides composed of a linear mannose backbone with galactose side groups. Their ability to greatly increase solution viscosity at low concentrations makes them valuable industrial polymers (Dumitriu, 2004; Prajapati et al., 2013). Locust bean gum (LBG), extracted from the seeds of the tree *Ceratonia siliqua*, is one of the most widely used galactomannans, commonly employed in the food industry as a thickener and stabiliser (Saha & Bhattacharya, 2010). It is also used in industrial applications such as textiles and cosmetics, and has shown potential in edible film manufacture, biopharmaceutical studies, nanoparticle synthesis, and soil stabilisation (Armistead et al., 2022; Barak & Mudgil, 2014; Cerqueira et al., 2011; Grenha & Dionísio, 2012; Perestrelo et al., 2014; Tagad et al., 2014; Ventura et al., 2015).

To produce LBG powder, carob seeds are first dehusked by either acid or mechanical treatment, and the endosperm is then separated from the germ and milled (Barak & Mudgil, 2014; Kawamura, 2016). The powder is typically light brown or yellow in appearance, and may contain dark specks from the husk (which can remain following incomplete separation), particles from the germ, and other impurities including fat, enzymes, and ash, as well as cellulose, lignin, and proteins from cell walls (Biliaderis & Izydorczyk, 2006; Coppen and Food and Agriculture Organization of the United Nations., 1995; Ellison et al., 2008; Newburger, 1961; Sébastien et al., 2014; Sutton et al., 1997).

Galactomannans are composed of a backbone of D-mannose units (connected by 1,4-linkages; M) and galactose substituents (connected by 1–6-glycosidic linkages; G), as illustrated in Fig. 1. The ratio of mannose to galactose units (M:G) varies with species, growing conditions, refinement protocols, and between individual chains within a given sample. The mannose backbone is essentially insoluble in water, while the galactose substituents increase solubility, making the molar M:G ratio an important characteristic which strongly affects solution behaviour (Gaisford et al., 1986; Picout et al., 2001; Prajapati et al.,

* Corresponding author.
E-mail address: k.j.l.mattsson@leeds.ac.uk (J. Mattsson).

https://doi.org/10.1016/j.carbpol.2023.121286
Received 13 May 2023; Received in revised form 4 August 2023; Accepted 9 August 2023
Available online 25 August 2023

2013). Highly substituted galactomannans (low M:G ratios) are more easily solubilised in water and less prone to aggregation than those with high M:G ratios. For LBG, M:G is typically ~ 3.5:1; other common galactomannans include tara gum (M:G ~ 3:1), guar gum (M:G ~ 2:1), and fenugreek gum (M:G ~ 1:1) (Prajapati et al., 2013).

As with other polymers, the molecular weight (M) of galactomannans strongly influences solution behaviour—governing for example the viscosity, frequency-dependent viscoelasticity, and the crossover values between viscosity-concentration regimes (Colby, 2010; Rubinstein & Colby, 2003). In turn, M will dictate processability, dispersion thickening effects, and textural characteristics, such that knowing the M distribution of a galactomannan sample is critical to understand and predict its behaviour in application. Reported values of M for LBG typically fall between ~300 and 2000 kDa ($3 \times 10^5 - 2 \times 10^6$ g mol^{-1}), with variation expected between samples due to the natural origins of LBG and differences in growing conditions (Barak & Mudgil, 2014).

One of the most commonly used methods for polymer molecular weight characterisation is size-exclusion chromatography coupled with multi-angle light scattering (SEC-MALS). Based on the use of a filtration-based solution preparation procedure, it has been previously suggested that SEC-MALS could produce reasonable values of M for LBG, tara gum, and guar gum (Picout et al., 2001; Picout et al., 2002). However, the authors of these studies noted that the polymer distributions showed unphysical scaling between M and R_g (radius of gyration), and suggested that only the distribution-averaged values (e.g. M_w and $R_{g,z}$) were reliable. The SEC chromatograms, MALS data, and full M and R_g distributions were not provided in these publications, making it difficult to assess the utility of the method, but the work to date suggests that it is difficult to use SEC-MALS to fully characterise the M and R_g distributions for galactomannans. Furthermore, it was stressed that large aggregates, which could influence solution behaviour, would not be observed by this method (Picout et al., 2001).

MALS, or static light scattering (SLS), may also be used to determine M without fractionation. Here, the scattering is determined across multiple angles for samples of varying polymer concentration, c; the weight-averaged molecular weight M_w is then determined in the low-c, low scattering angle limit (Rubinstein & Colby, 2003). For LBG (and other galactomannans), however, this method is often problematic due to the presence of aggregates, which cause an excess in scattering intensity at low angles, affecting the extrapolations used in the analysis (e.g. Zimm plots) (Doublier & Launary, 1981; Gaisford et al., 1986). Our recent work demonstrated the presence of 'excess' scattering from aggregates in aqueous LBG solutions down to wavevectors as low as 0.07 μm^{-1}, by the use of ultra small angle light scattering (USALS). The investigated solutions were filtered during preparation, using 1.2 μm diameter pore-size filters; yet, the results suggest the presence of aggregates larger than ~ 14 μm (O'Connell et al., 2023). Thus, it appears difficult to fully avoid the presence of aggregates, demonstrating that the utility of SLS for characterisation of the well-dispersed LBG will generally be limited.

Another alternative, and simpler, M determination method is based on the intrinsic viscosity ($[\eta]$). $[\eta]$ is related to molecular weight by the Mark-Houwink relation: $[\eta] = KM^{\alpha}$, where K and α are parameters specific to the investigated polymer-solvent system (Rubinstein & Colby, 2003; Young & Lovell, 2011). This method thus requires K and α to be known for LBG in water. It has been noted that other, more easily dispersed, galactomannans—such as guar and tara gums—show similar conformation to LBG in water; thus, measurements on these gums may also be used to calculate appropriate Mark-Houwink parameters (Picout et al., 2002; Picout & Ross-Murphy, 2007). A review of multiple $[\eta]$-M datasets for guar gum, alongside data for LBG and tara gums, showed no significant differences in the Mark-Houwink parameters between the galactomannans, showing that the same parameters can be used with some confidence for all three galactomannans and potentially also for other galactomannans with similar M:G ratios (Picout & Ross-Murphy, 2007). A general challenge with this M determination method is to achieve an accurate measurement of the difference in viscosity between the dilute polymer solutions and the solvent alone (e.g. water). Furthermore, for galactomannans such as LBG, the viscosity of the dilute solutions may be affected by aggregation, which could lead to errors in the determined value of M.

Each of the three approaches, discussed above, has limitations for galactomannan characterisation, and notably none of the methods appear capable of reliably measuring the full M (or R_g) distribution. We hypothesise that the use of an alternative technique, asymmetric flow field-flow fractionation (AF4) coupled with MALS, refractive index (RI), and UV/VIS detectors, will allow for a complete characterisation of LBG solutions, including size, molecular weight, and conformation of dispersed and aggregated fractions, without the problems faced by other techniques. AF4 achieves separation between polymeric species by subjecting samples to a laminar elution flow of parabolic profile within a thin channel, together with a concurrent 'cross-flow' perpendicular to the direction of the elution (Cölfen & Antonietti, 2000). The cross-flow first directs solutes to a membrane forming the lower wall of the channel, and is then reduced in flow strength to allow diffusion back towards the channel center, where solutes are subject to stronger elution flow. In this geometry, the rate of solute diffusion is inversely proportional to their hydrodynamic size; thus, smaller solutes move further from the wall, experience greater elution flows, and thus elute earlier than larger solutes. This separation process ensures that very low shear rates are exerted upon the sample—making the method ideally suited for the characterisation of high molecular weight linear and branched polymers which may exhibit degradation under the conditions experienced in

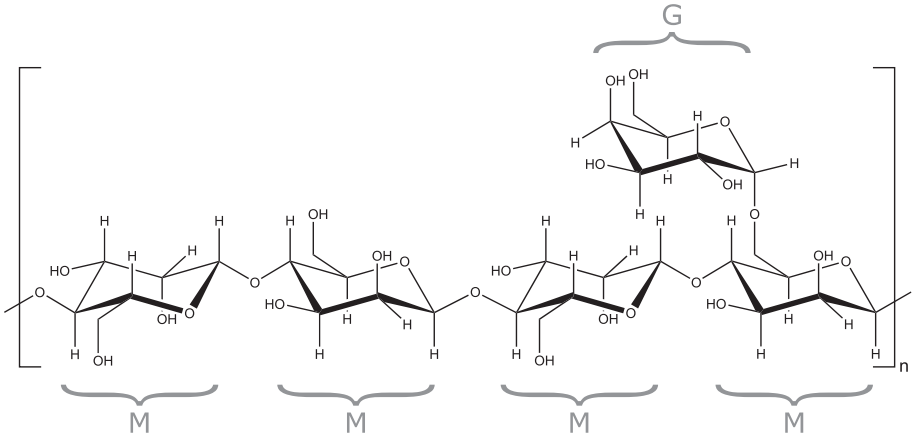

Fig. 1. Chemical structure of LBG, showing a representative section of the mannose (M) backbone with a single galactose (G) side unit.

SEC, leading to inaccurate determinations of mass, radii, and conformation (Makan et al., 2012; Otte et al., 2011; Woo et al., 2016). Furthermore, these benefits also make the method suitable for the separation of dispersed and aggregated polymer fractions, without the loss of the latter, as has recently been demonstrated for chitosan (González-Espinosa et al., 2019).

Our AF4 characterisation confirms the presence of aggregates, demonstrating that LBG solutions should be considered mixtures of dispersed and aggregated polymer fractions. We determine the distributions of molar mass and radius of gyration for both polymer fractions, and the relation between the two provides insight regarding the polymer conformation. We also explore the use of varying filtration procedures, and show that the aggregates can be effectively removed by using a filter of appropriate membrane material with sufficiently small pore size. Furthermore, we prepare solutions of nearly fully-dispersed LBG at a range of concentrations via this protocol, and perform static (SLS) and dynamic (DLS) light scattering measurements on these for comparison to our previous study on LBG solutions containing aggregates (O'Connell et al., 2023). Finally, we demonstrate that the nature of both the dispersed and aggregated fractions may be significantly modified by changes to the solvent conditions.

2. Materials and methods

2.1. Source material

Locust bean gum was sourced from LBG Sicilia (Seedgum C-175S). The M:G ratio for this sample has previously been determined as (3.4 ± 0.3):1 using polarimetry, and the molecular weight estimated as $M_w = 1.7 \pm 0.5 \times 10^6$ g mol^{-1} via intrinsic viscosity measurement, though it should be noted that careful molecular weight determination is a focus of the present work using AF4 (O'Connell et al., 2023).

Seedgum C-175S is a commercial LBG product typical of the quality used in many industrial applications. It is manufactured using a chemical-free process, using mechanical treatments to dehusk the seeds, separate the endosperm and germ, and grind the endosperm into a powder. In appearance, the gum is a light brown powder with visible brown specks.

2.2. Solution preparation

Stock solutions at 0.25 wt% LBG were prepared by dispersing LBG powder in Milli-Q water under stirring (the water was additionally filtered twice through 200 nm pore size nylon membrane syringe filters), first at room temperature, and then at 85°C for 45 min (still under stirring). Subsequently, the dispersions were left to cool to room temperature, after which they were stirred for another 30 min. The stock solutions were then diluted to 0.05 wt% and left to stir overnight.

The solutions were initially filtered using 5.0 μm, followed by 1.2 μm, pore diameter surfactant-free cellulose acetate (SFCA) membrane syringe filters. The final concentration of the solutions was determined as 0.041 wt%, by drying, followed by weighing of the dried powder. Subsequently, the solutions followed three alternative preparation procedures: (i) no additional filtration (denoted as 1200-SFCA), (ii) additional filtration through a 200 nm pore diameter regenerated cellulose (RC) membrane syringe filter (denoted as 200-RC), or (iii) additional filtration through a 200 nm pore diameter nylon membrane syringe filter (denoted as 200-NYL).

For the concentration-dependent SLS and DLS measurements only, samples were prepared at six concentrations (ranging from 0.018 to 1.1 wt%) following the 200-NYL protocol, by either dilution or concentration of the stock. Dilutions were carried out by mixing filtered stock and water in a vial, which was agitated using a vortex mixer for one minute and left to rest overnight before measurement. Drying to reach higher concentrations was achieved by rotary evaporation of filtered stock in a round-bottom flask (120 mPa, 57°C, 70 rpm).

To explore the effect of increased ionic strength and pH on LBG, solutions were also prepared following the 1200-SFCA protocol, but with modified solvent conditions at all stages of the preparation, consisting of: (i) 0.1 M sodium nitrate ($NaNO_3$) and 0.02 wt% sodium azide (NaN_3) (denoted as NITR), and (ii) 50 mM phosphate buffer solution (pH = 8) (denoted as PHOS). The solutions in both cases were prepared using Milli-Q water, filtered twice through 200 nm pore size nylon membrane syringe filters prior to use. Samples were filtered using 5.0 μm, followed by 1.2 μm, surfactant-free cellulose acetate (SFCA) membrane syringe filters, as in the 1200-SFCA protocol. The solution preparation protocols are illustrated in Fig. 2.

2.3. Asymmetric flow field-flow fractionation (AF4)

AF4 measurements were performed using an AF2000 multiflow system from Postnova Analytics (Malvern, UK). The system was coupled with an online 21 angle multi-angle light scattering (MALS) detector (PN3621), a refractive index (RI) detector (PN3150), and a dual wavelength UV detector (PN3211) set at 220 and 280 nm. The system was equipped with an analytical asymmetric AF4 channel (Postnova *Z*-AF4-CHA-611) using a 350 μm spacer; the membrane used was made from regenerated cellulose fibres with a 10 kDa cut-off. Solutions were injected at a concentration of 0.041 wt%, and the injected volume for each measurement was 50 μL.

The cross-flow profile used is shown in Fig. 3, composed of a focusing

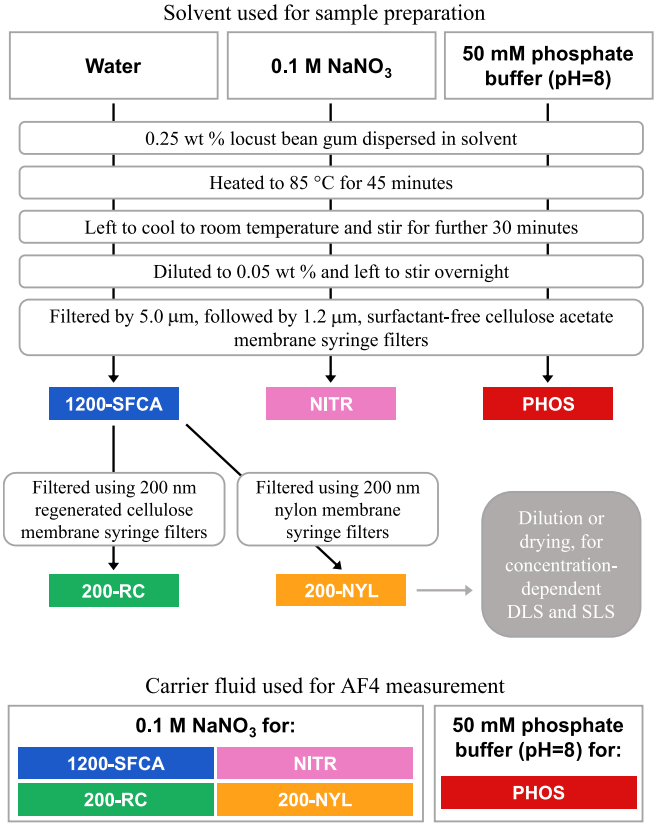

Fig. 2. The five protocols followed to prepare LBG solutions for AF4 characterisation: '1200-SFCA' (final filtration: 1200 nm surfactant-free cellulose acetate membrane), '200-RC' (final filtration: 200 nm regenerated cellulose membrane), '200-NYL' (final filtration: 200 nm nylon membrane, additionally prepared at a range of concentrations for 'bulk' SLS and DLS measurements without fractionation by AF4), 'NITR' (filtration as in 1200-SFCA; prepared in water with added nitrate), and 'PHOS' (filtration as in 1200-SFCA; prepared in phosphate buffer). The lower section indicates the carrier fluid used for AF4 measurements for each of the protocols.

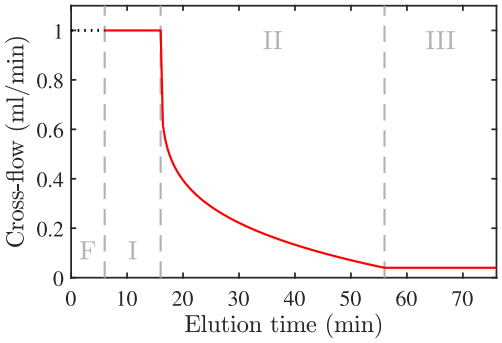

Fig. 3. Cross-flow profile, showing the focusing step (F) and elution stages (I-III). The cross-flow decays from 1 to 0.04 mL min^{-1} during elution stage II.

stage and three elution stages. The focusing stage had a cross-flow of 1 mL min^{-1} for 6 min, with a focus pump flow of 1.3 mL min^{-1}. The first elution stage maintained the cross-flow at 1 mL min^{-1} for 10 min; the second reduced the cross-flow to 0.04 mL min^{-1} over a period of 40 min, decreasing as a power of time with exponent 0.2; and the third maintained cross-flow at 0.04 1 mL min^{-1} for 20 min.

Initial measurements were made on 1200-SFCA samples, using a carrier liquid of ~ 0.1 M sodium nitrate ($NaNO_3$) and ~ 0.02 wt% sodium azide (NaN_3). Measurements on 200-NYL, 200-RC, and NITR samples were performed in the same carrier liquid, while 50 mM phosphate buffer solution (pH = 8) was used as the carrier liquid for PHOS samples (the solvent used in their preparation).

The MALS system allowed simultaneous measurement of scattering intensity at multiple values of the scattering wavevector, $q = (4\pi n/\lambda_0)sin(\theta/2)$, where n is the sample refractive index, λ_0 is the vacuum wavelength of the incoming light, and θ is the scattering angle (the angle between the incoming and scattered light). Scattering profiles were corrected to account for solvent contributions, variations in incoming laser intensity, scattering volume, and detector properties etc. by conversion to the excess Rayleigh ratio, $\Delta R(q)$:

$$\Delta R(q) = \frac{I(q) - I_s(q)}{I_{ref}(q)} \left(\frac{n}{n_{ref}}\right)^2 R_{ref}, \quad (1)$$

where $I_s(q)$ is the solvent scattering intensity (recorded in a blank carrier fluid measurement), and $I_{ref}(q)$, n_{ref}, and R_{ref}, are respectively the measured scattering intensity, refractive index, and Rayleigh ratio of a reference sample (Berry & Cotts, 1999; Schärtl, 2007).

The profiles were analysed to determine the radius of gyration, R_g, and molecular weight, M, as a function of elution time using integration windows of ~ 3 s. R_g and M were determined by plotting the data in the form of a Debye plot ($\Delta R/Kc$ against $sin^2(\theta/2)$, where $K = (4\pi^2 n^2)(dn/dc)^2/(N_A\lambda^4)$ (the optical constant) and c is the concentration). Subsequently, data were fitted using the Debye scattering function, which describes the scattering from Gaussian random coils (Debye, 1947):

$$\Delta R(q) = \frac{2I_0}{x^2}[e^{-x} - (1-x)]. \quad (2)$$

Here, I_0 is the amplitude of the scattering intensity, and $x = \left(qR_g\right)^2$. In a Debye plot M is given by the value of $\Delta R/Kc$ at $\theta = 0$, i.e. the intercept of the ordinate for zero value of the abscissa (examples are shown in Fig. 5). R_g, in turn, is determined as $(\lambda_0/\pi n)\sqrt{(3M/16)m_{q=0}}$, where $m_{q=0}$ is the slope of the fit at zero scattering angle (Andersson et al., 2003). The polymer concentration during elution was determined from the RI signal, using a refractive index increment of $dn/dc = 0.15$ mLg^{-1}, consistent with previously used and experimentally determined values for LBG (Richardson et al., 1998; Richter et al., 2004; Sébastien et al., 2014). For each sample, repeats were made to ensure reproducibility, and a representative run was chosen to display in figures comparing protocols (repeat data for RI, R_g, and M are shown in Figs. S1 and S8 (SI)).

2.4. Static and dynamic light scattering

Dynamic (DLS) and static (SLS) light scattering measurements were performed on 200-NYL samples, at six LBG concentrations within the range of 0.018 to 1.1 wt%. Measurements were performed using a photon correlation spectrometer (LS Instruments AG, Switzerland) with a diode-pumped solid-state laser of vacuum wavelength $\lambda_0 = 660$ nm. Samples were placed in 10 mm diameter glass cuvettes, and were left in position for at least 30 min before measurements were performed. All measurements were made at 25 °C.

A detector goniometer was used to perform measurements for scattering angles in the range of 24 to 110°, corresponding to scattering wavevectors in the range of 5.3 to 20.7 μm^{-1}. For SLS analysis, the excess Rayleigh ratio ($\Delta R(q)$) was calculated as in Eq. 1, with toluene as the reference sample and using a literature value of R_{ref} for toluene at $\lambda = 660$ nm (Wu, 2010). Measurements were performed in a pseudo-cross correlation mode, allowing calculation of the intensity autocorrelation function, $g_2(\tau)$, without detector after-pulsing artifacts at short lag times (Schätzel, 1987). Data were fitted in the form $(g_2(\tau) - 1)/\sigma$, where σ is the coherence factor, set by the specifics of the scattering set-up (Borsali & Pecora, 2008).

3. Results and discussion

In the following subsection we explore the effect of filtration on aqueous LBG solutions, presenting AF4 results for samples prepared using the different filtration protocols (1200-SFCA, 200-RC, and 200-NYL). Samples prepared with the 200-NYL protocol are observed to consist almost entirely of dispersed polymer, without an aggregated fraction. To investigate the dispersed polymer fraction in more detail, we thus perform a concentration-dependent study of these samples using SLS and DLS experiments, as presented in Section 3.2. Finally, in Section 3.3, we present AF4 results for the LBG solutions in modified solvent conditions (comparing the 1200-SFCA protocol, using water, to NITR and PHOS).

3.1. Effect of solution filtration

3.1.1. AF4 elution profiles for the three filtration protocols

Representative AF4 elution profiles based on refractive index, MALS signals at 90 and 20°, and UV absorption at 280 nm are shown in Fig. 4, for solutions following the 1200-SFCA, 200-RC, and 200-NYL protocols (with the AF4 carrier fluid in all cases being 0.1 M sodium nitrate ($NaNO_3$) and 0.02 wt% sodium azide (NaN_3)). Following the 1200-SFCA protocol, three elution peaks can be identified: (i) a broad peak spanning ~ 20–50 min, most clearly observed in the refractive index (RI) and MALS at 90°, but also present at a much lower relative magnitude in the MALS at 20° (see Fig. 4d); (ii) a narrower peak at ~ 47–54 min, most apparent in the UV absorption and in both MALS signals; and (iii) a third peak, of similar breadth to (ii) and also clearly observed both in the UV and MALS signals, but at slightly longer elution times (~ 55–60 min). Peaks (ii) and (iii) are more clearly distinguished in the MALS signal at 20°, whereas at 90° they are not well resolved and appear as one effective broad contribution.

Using AF4, objects with increasing hydrodynamic radii elute at progressively longer times. We therefore expect the material eluted in the peaks (i), (ii), and (iii) to have progressively larger hydrodynamic radii. Additionally, the scattering associated with peaks (ii) and (iii) dominates that of peak (i) at 20°, while having more comparable magnitudes at 90°, suggesting objects with a larger radius of gyration (the angular dependence of the scattering is explored in more detail later). We therefore identify the peaks as the elution of well-dispersed LBG

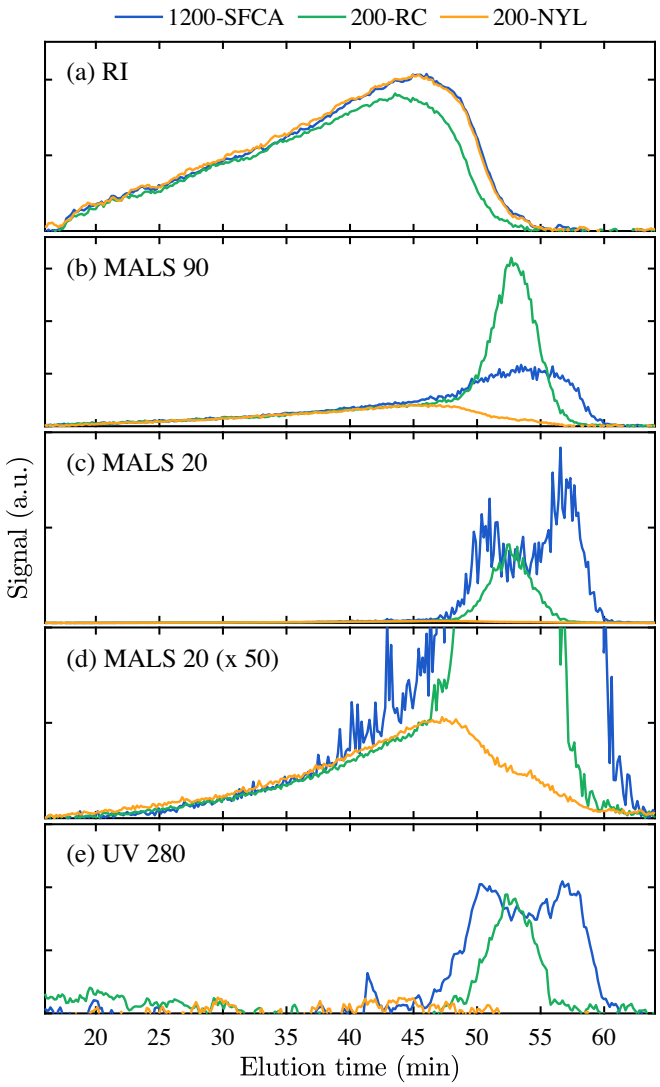

Fig. 4. AF4 elution profiles for LBG solutions with various filtration treatments following the standard preparation protocol (1200-SFCA: no additional filtration; 200-RC: 200 nm regenerated cellulose filtration; and 200-NYL: 200 nm nylon filtration): (a) refractive index, (b) MALS at 90°, (c) MALS at 20°, (d) MALS at 20° scaled by a factor of 50, and (e) UV absorption at 280 nm.

molecules, followed by the elution of two aggregated fractions, somewhat separated in size.

While the MALS signals clearly show the elution of both well-dispersed polymer and aggregates, the RI signal closely follows the dispersed polymer elution and shows, at most, a very small contribution from the aggregates, suggesting they comprise a marginal portion of the sample by mass. In contrast, the UV absorption at 280 nm reflects only the aggregate elution, coinciding with peaks (ii) and (iii) in the MALS signals. Absorption at this wavelength is typically associated with the aromatic amino acids tryptophan and tyrosine—indicating the presence of protein, as exploited for protein content determination in the A280 assay (Edelhoch, 1967; Schmid, 2001). The UV absorption therefore suggests the presence of residual protein which appears strongly associated with the aggregates. This raises interesting questions regarding the composition and formation of these aggregates, and the role that residual protein might play. Aggregation can be driven by attractive interactions such as hydrogen bonding and hydrophobic interactions between proteins and/or polysaccharides (Gentile, 2020; McClements, 2006). Protein aggregation is particularly likely following thermal denaturation, which may well be the case in our samples given the solubilisation at 85°C (Cochereau et al., 2019; Gentile, 2020; Liu et al., 2021). Notably, our data do not explicitly show to what extent the aggregates consist of galactomannan. If the protein composition had been known, it might have been possible to use a reference standard to calibrate the UV detectors and quantify protein concentration during elution; LBG powders have previously been shown to contain a mix of structural proteins and enzymes, as well as impurities from the highly proteinaceous germ, though the exact composition will vary between samples (Lopes da Silva & Goncalves, 1990; McCleary & Matheson, 1974, 1975). In future work, it would be interesting to investigate further the composition and origin of the aggregates, though this is outside the scope of the present work. Evidence for galactommanan association in the absence of protein will be presented in Section 3.2.

The 200-RC protocol, which includes an additional filtration through a 200 nm regenerated cellulose membrane, leaves the RI signal unchanged up to 35–40 min, but has a noticeable effect at longer elution times (Fig. 4a), indicating partial removal of the highest molecular weight dispersed chains. The MALS data (for both scattering angles) and UV absorption show only a single elution peak in the region where peaks (ii) and (iii) were observed for 1200-SFCA samples, indicating that the aggregate fraction is significantly changed by the additional filtration. This aggregate elution appears closer to 1200-SFCA peak (ii), suggesting the filtration removes the largest aggregates from the solutions.

Considering the 200-NYL protocol, which includes an additional filtration through a 200 nm nylon membrane, only the dispersed elution contribution is observed. Aggregate contributions are not detected in any of the signals, including MALS at 20° which is highly sensitive to the presence of aggregates; this suggests that the supramolecular aggregates are nearly completely removed by the nylon filtration. The residual protein was also removed, as indicated by the lack of any detectable UV absorption (Fig. 4). Indeed, nylon filtration membranes are known to strongly bind protein, while cellulosic membranes do not (Joshi & Chernokalskaya, 2011). Notably, despite this significant difference, the 200-NYL and 1200-SFCA MALS profiles are remarkably similar across the dispersed fraction elution (peak (i)), and the RI profiles are practically indistinguishable across the entire elution, indicating that the stricter filtration has a minimal effect on the dispersed polymer fraction. In the MALS signals, the removal of the aggregates and their dominant scattering contribution renders observable the elution of the largest dispersed LBG molecules, allowing for a more complete characterisation of the dispersed polymer distribution.

3.1.2. *Determination of R_g and M*

To find the radius of gyration (R_g) and molecular weight (M) as a function of elution time, the MALS data were plotted as $\Delta R/Kc$ versus $sin^2(\theta/2)$, where the concentration (c) was determined from the RI signal; thus, these parameters are only reliably determined when the RI signal is sufficiently strong. The data were fitted using the Debye random coil scattering model (Eq. 2); R_g was then determined from the intercept of the ordinate, and M from the slope of the data at $\theta = 0$. Examples of the fitting are shown in Fig. 5 for elution times of 23, 33, 43, and 53 min. This approach described the data well during the dispersed polymer elution (23, 33, and 43 min), but was less successful for the aggregate fraction (e.g. 53 min), though still capturing the core features of the data. Other scattering models (polynomial extrapolation following the Zimm, Debye, or Berry methods, as well as the hard sphere model) were also investigated, but did not lead to significant improvements. Thus, the Debye scattering model was used at all elution times for consistency. R_g and M are shown in Fig. 6 for elution times during which the RI signal (see Fig. 4) was non-negligible. Repeat data for each protocol are shown in Fig. S1 (SI).

For the 1200-SFCA sample, both R_g and M increase steadily throughout the dispersed polymer elution, showing an LBG distribution with molecular weights from $\sim 3 \times 10^5 - 1.5 \times 10^6$ g mol^{-1} and radii of gyration from $\sim$ 30 to 100 nm. Beyond $\sim$ 47 min, both R_g and M increase

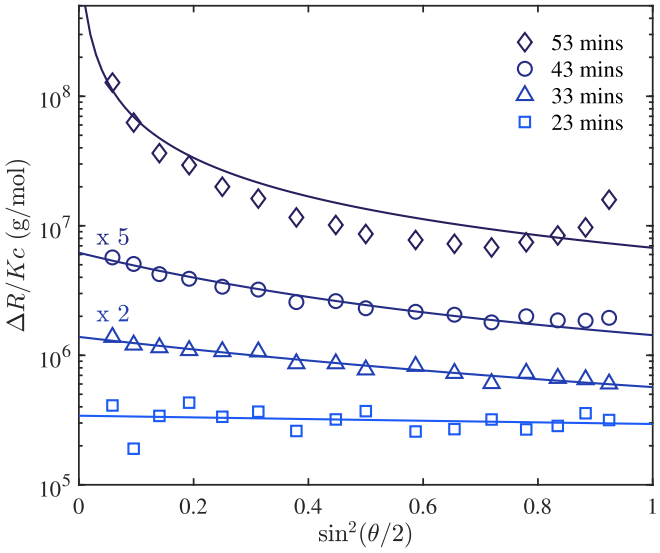

Fig. 5. A Debye plot showing data for four representative elution times from a 1200-SFCA sample. Solid lines are fits to the Debye random coil scattering model (Eq. 2). Data for 33 and 43 min are scaled by factors of 2 and 5, respectively, for clarity.

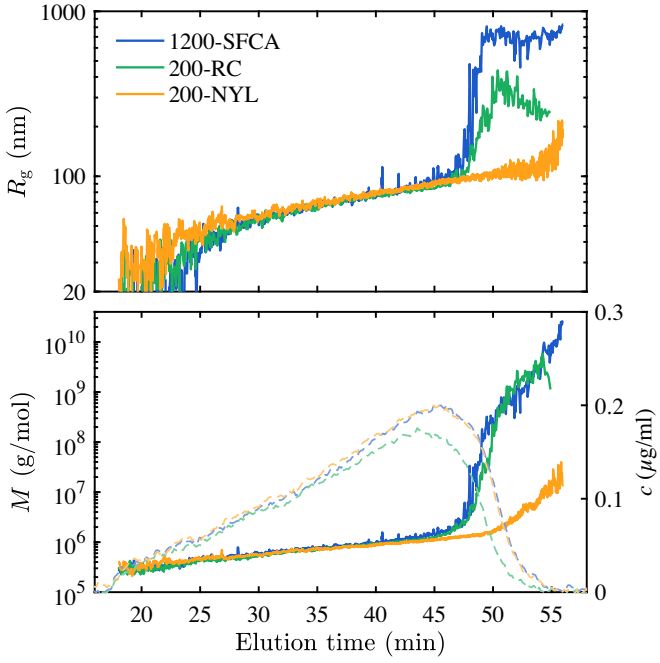

Fig. 6. Profiles of R_g and M against elution time determined by AF4-MALS measurements for LBG solutions following various filtration treatments. Dashed lines overlaying the M data show the concentration elution profiles.

significantly, reflecting the start of the aggregate elution. From ~ 49 min, the data stabilise somewhat, with R_g in the range of ~ 600–800 nm and M at $\sim 2\times10^8 - 2\times10^{10}$ g mol^{-1}, providing estimates of the aggregate size and mass. Values of $R_g \lesssim 30$ nm show high levels of noise and should not be considered reliable; the scattering for objects of this small size has a very weak angular dependence (as illustrated e.g. by the 23 min elution time data in Fig. 5), leading to significant relative uncertainties in the slope, and thus R_g. In contrast, the M data—determined using the y-intercept—are significantly more robust.

For the 200-RC sample, the R_g and M data for the dispersed fraction are almost identical to those without additional filtration. In contrast, the aggregate fraction shows a reduction in radius while the molar mass is largely unchanged; this suggests that the aggregates are compressed to a smaller size during filtration, as opposed to being broken into smaller aggregates, where a reduction in molar mass would also be expected.

For the 200-NYL sample, the results for the dispersed fraction are again almost identical. However, the increase in R_g at long elution times has almost entirely disappeared, and only a small increase in M is observed for the longest elution times, beyond ~ 51 min, by which point the RI elution signal has essentially ended; this contrasts the 1200-SFCA and 200-RC samples, for which the increases in R_g and M occur while the RI elution is still significant.

Considering the operating principle of AF4, it may seem surprising that (1) aggregates of several hundred nanometers elute at similar retention times to dispersed polymer of ~ 100 nm (see Fig. 6), and (2) the small remaining aggregate fraction in the 200-NYL data elutes at longer times than those removed by filtration, despite the presumed larger size of the latter. We suggest that these observations are caused by a transition to an inverse (steric or hyperlayer) elution mode as a critical solute size is reached, under which retention time decreases with increasing hydrodynamic size (see Appx. C (SI)) (Kowalkowski et al., 2018; Myers & Giddings, 1982). Indeed, this transition has been observed for critical sizes of 400–600 nm for polystyrene particles and branched cationic polyacrylamide measured in similar setups (Kim et al., 2018; Woo et al., 2016). In future measurements, it may be possible to achieve a more complete separation of dispersed and aggregated fractions by further optimization of parameters such as spacer thickness and cross-flow profile.

In summary, the AF4 method allowed the separation and identification of dispersed and aggregated fractions in dilute LBG solutions. Where present, the aggregate fraction masked the upper end of the dispersed elution, preventing full characterisation of molecular weight and radii distributions. The aggregates were effectively removed by additional filtration through a 200 nm pore size nylon membrane, while they were modified—but not removed—by a regenerated cellulose membrane of the same pore size. The dispersed fraction remained remarkably similar between all three protocols; thus, the nylon filtration procedure was shown to allow a more complete characterisation of well-dispersed LBG, having removed the aggregates without affecting the dispersed fraction distribution.

3.1.3. *Distribution-averaging of R_g and M*

To determine average values of R_g and M, the data shown in Fig. 6 may be integrated over the relevant range of elution times. A challenge lies in choosing appropriate upper integration limits: one wishes to capture the dispersed polymer fraction as fully as possible, while avoiding contributions from the aggregate elution which lead to greatly skewed average values. We employ a simple and practical approach to evaluating these effects, which is to plot the resulting averages as a function of the chosen upper integration limit: this is illustrated for 1200-SFCA and 200-NYL samples in Fig. 7. To track the elution progress, the portion of the total injected solute mass that has eluted (the recovery) is also shown (calculated as the integral of concentration over the chosen time range, divided by the known injected mass (20.5 μg)).

For the 1200-SFCA sample, the resulting values increase gradually as the upper integration limit increases, as more of the LBG distribution is included, up to ~ 48 min; beyond this, the aggregate contribution skews the results. The effect is dramatic for intensity-averages and leads to significant errors in weight-averages, while the number-averaged data are almost unaffected and reach a plateau concurrent with the plateau in recovery. Thus, the LBG distribution can be well characterised in terms of number-averaged mass and radius of gyration, with M_n and $R_{g,n}$ of 9.1×10^5 g mol^{-1} and 59 nm respectively, but much less accurately by weight or intensity averages.

Following the 200-NYL protocol, the significant upturn at ~ 48 min is not observed in any of the averaging methods, and these all approach

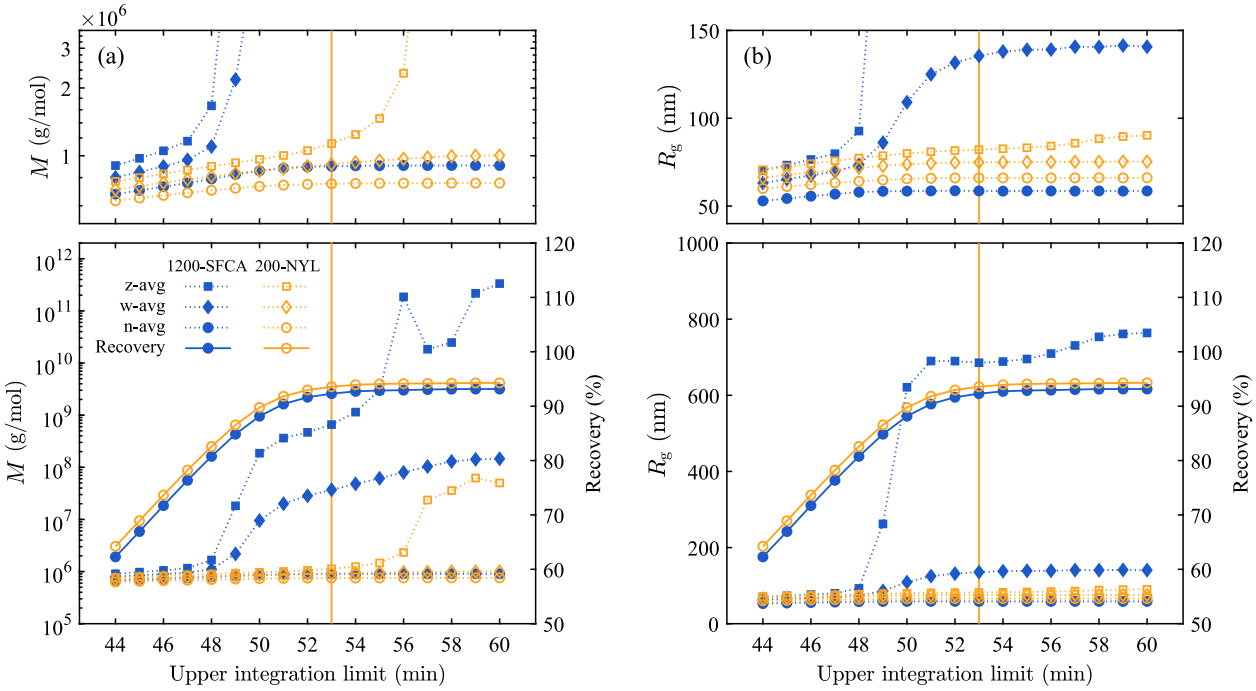

Fig. 7. Molecular weight (a) and radius of gyration (b), averaged by intensity (z-avg), weight (w-avg), and number (n-avg), as a function of the chosen upper integration limit (with the lower integration limit fixed at 18 min). The mass recovery over the same integration window is also shown. Vertical lines denote 53 min—the chosen upper limit for which values are reported in the text.

plateau values. Beyond ~ 54 min, the small remaining aggregate fraction causes upturns in the intensity-averaged data; this is very slight for $R_{g,z}$, but more significant for M_z for which the data do not reach a plateau prior to the upturn. The number and weight-averaged data (for both R_g and M) reach very clear plateaus coinciding with the recovery plateau. Thus, the LBG distribution can be properly described by all three averaging methods. Using an upper elution time limit of 53 min, the resulting molecular weight values were: $M_n = 7.5 \times 10^5$ g mol^{-1}, $M_w = 9.2 \times 10^5$ g mol^{-1}, $M_z = 1.1 \times 10^6$ g mol^{-1}, with a dispersity of $M_w/M_n = 1.22$ and a mass recovery of 94 %. The radius of gyration values were: $R_{g,n} = 66.0$ nm, $R_{g,w} = 74.9$ nm, and $R_{g,z} = 82.1$ nm.

For comparison, we previously determined the molecular weight of the same LBG powder as $M_w = (1.7 \pm 0.5) \times 10^6$ g mol^{-1}, using intrinsic viscosity measurement and Mark-Houwink parameters from literature (O'Connell et al., 2023; Picout et al., 2002); this was also used to estimate $R_{g,w}$ as 92 ± 9 nm, using the Flory-Fox relation. Comparing these values to the AF4 determination ($M_w = 9.2 \times 10^5$ g mol^{-1}, $R_{g,w} = 74.9$ nm), we find that the values based on intrinsic viscosity are somewhat larger than expected, which could be due to a small intrinsic viscosity contribution from the aggregates. However, we note that the M_w values obtained with upper integration limits that avoid the aggregate fraction (e.g. 44–47 min) are higher for the 1200-SFCA protocol than for the 200-NYL protocol (Fig. 7a), and it seems likely that they would reach values of 1.2×10^6 g mol^{-1} or slightly higher if the full dispersed polymer fraction could have been observed—consistent with the determination from intrinsic viscosity.

The average M, R_g, and recovery values are provided for each of the protocols in Table S1 (SI); results from integration over regions representing both the dispersed and aggregated fractions are given, as well as over the entire observed elution to determine total mass recovery. If the dispersed fraction integration is cut at 45 min, fairly consistent values are found across the filtration protocols. As discussed above, the integration may be extended up to 53 min following the 200-NYL protocol, thus more completely representing the dispersed polymer fraction while avoiding effects from the aggregates; for the other protocols, integration to this limit provides greatly skewed values for the dispersed fraction. The total recovery of the 200-RC protocol is around 15 % lower than those of 1200-SFCA and 200-NYL (81 % compared to 95 %), confirming the removal of material by this filtration.

3.1.4. Polymer conformation

The determined R_g and M may be used to construct a 'conformation plot', as shown in Fig. 8, by matching the R_g and M at each elution time. Here, we excluded data within the elution time range for which the dispersed polymer and aggregate fractions overlap, since these are not

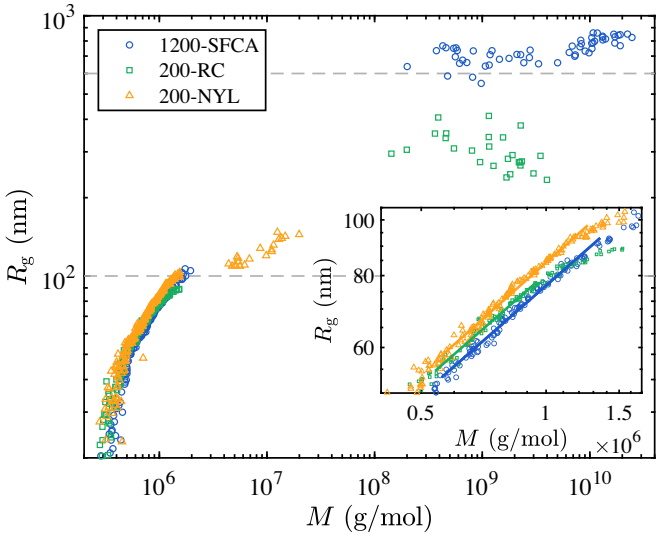

Fig. 8. Conformation plot of R_g versus M, based on AF4-MALS data. Dashed lines mark the filtration pore radii used in the three protocols: 600 nm, as used in 1200-SFCA, and 100 nm, as used in 200-RC and 200-NYL. The inset shows an expanded view of the fitted region; solid lines are linear fits to the data they span, with slopes of $\nu = 0.63 \pm 0.01$ for 1200-SFCA, $\nu = 0.63 \pm 0.01$ for 200-RC, and $\nu = 0.64 \pm 0.01$ for 200-NYL.

directly representative of one particular structure (the excluded times are 46.4–50.0 min for the 1200-SFCA and 200-RC samples, and 50.0–52.5 min for 200-NYL). As shown in Fig. 8, for each of the protocols, two separate regions are clearly identifiable, corresponding to the dispersed and aggregated LBG fractions, respectively. The dispersed fractions show highly similar R_g–M scaling (although with some variation in the absolute values of R_g for any given M), while the aggregated fraction shows clear differences between the three protocols.

For the dispersed fraction, across an R_g range of roughly $50 - 90$ nm, an approximate power law behaviour is observed ($R_g \sim M^{\nu}$; thus, the behaviour is linear in a double logarithmic representation), suggesting the presence of a self-similar fractal structure. This is expected for a polymer solution lacking any structural transitions for increasing M, and the slope of the data corresponds to the Flory exponent (ν), providing information about the dispersed polymer conformation (de Gennes, 1979; Rubinstein & Colby, 2003). Power laws were fit to the data within this range, to determine the approximate scaling exponent for each of the protocols: $\nu = 0.63 \pm 0.01$ for 1200-SFCA, 0.63 ± 0.01 for 200-RC, and 0.64 ± 0.01 for 200-NYL. Thus, the dispersed polymer conformation is consistent following all three preparation methods. Moreover, the values are close to that predicted by the Zimm model for neutral flexible linear polymers in good solvent conditions ($\nu = 0.588$; c.f. 0.5 for θ conditions), with the slight enhancement suggesting a marginally more extended conformation ($\nu = 0.63$ corresponds to a fractal dimension of 1.59; c.f. 1.7 for good solvent conditions, 2.0 for a θ-solvent) (Rubinstein & Colby, 2003).

Conformation plots (R_g vs M) have previously been constructed for galactomannans using SEC-MALS, but unphysically low values of the Flory exponent were found when the full $R_g - M$ distributions were analysed (Picout et al., 2001, 2002). The authors were therefore limited to using the overall moments (distribution-averaged R_g and M values) determined for a series of samples prepared via thermal degradation. Following this approach, the authors found $\nu = 0.57 \pm 0.05$ for LBG, roughly consistent with our determination. Providing that the samples produced through degradation are to a good approximation homologous, this is a reasonable alternative approach, though highly labour-intensive. In contrast, the AF4 method provides the full $R_g - M$ distribution, allowing determination of ν from a measurement of a single sample. We do note, however, that our data span less than an order of magnitude in both R_g and M, so the resulting ν should be treated with some caution. A series produced through degradation may span wider R_g and M ranges, and thus provide more reliable values of ν.

For R_g below roughly 45 nm, the data for all three samples 'fall off' at an unphysically high slope of ~2. This may be related to the errors in sizing for these near-isotropic (near-independent of the scattering angle) scatterers (the lowest physical fractal dimension for a mass fractal in a connected structure is 1, corresponding to a maximum Flory exponent of $\nu = 1$ (Martin & Hurd, 1987)). At the upper end of the dispersed fraction, above ~ 95–100 nm, the 1200-SFCA and 200-NYL data flatten out, departing slightly from the power law scaling (see the inset to Fig. 8); this suggests that the largest molecules exhibit more compact conformations. For 200-RC, this effect is more pronounced and starts at around 85 nm, suggesting that the largest dispersed molecules were compressed by filtration and were not subsequently able to swell into a more expanded conformation.

Next considering the aggregated fraction, the data for the 1200-SFCA sample spans two orders of magnitude in mass, from $\sim 2 \times 10^8 - 3 \times 10^{10}$ g mol^{-1}, while showing a relatively constant radius of ~ 700 nm. Comparing this to the filtration pore radius of 600 nm, it is likely that the solution prior to filtration contained a broad distribution of aggregates which were then broken or compressed by filtration. The similarity between the size of the aggregates and the filter pore size, across a very wide range of molecular weights, suggests that the aggregates undergo a level of compression during filtration. Our previously reported SLS and USALS measurements for LBG, which used the same preparation protocol, revealed two aggregate populations: primary aggregates with a radius of 670 ± 140 nm, and secondary aggregates with radii of at least 14 μm (O'Connell et al., 2023). The primary aggregate mass was estimated as 1.5×10^{10} g mol^{-1}, using a Zimm analysis of light scattering data (O'Connell et al., 2023). The aggregate fraction observed by AF4 appears highly consistent with the primary aggregates observed in the bulk solution scattering measurements.

Following the 200-NYL protocol, the aggregates were largely removed. The small remaining fraction are greatly reduced in both mass and radius, with radii of ~ 110–150 nm. The large reduction in mass suggests that aggregates are broken during filtration, and the observed radii could be understood as a result of slight re-aggregation and/or swelling of aggregates after filtration (c.f. the pore radius, 100 nm).

In contrast, the aggregate fraction of the 200-RC sample has a lower mass compared with that of the 1200-SFCA sample, and its radius is reduced to ~ 300 nm. The mass and radius are both, however, significantly higher than for the 200-NYL sample. Thus, it appears either that re-aggregation occurs following filtration using regenerated cellulose membranes, and/or that this type of filter results in aggregates that are able to swell to a size notably larger than the filter pore size. Recalling the association between the aggregated fraction and residual protein, and that the protein was removed by the 200-NYL protocol but not 200-RC, it seems plausible that this difference in sample composition may lead to re-association. Overall, the differences between the results for the two types of 200 nm filters demonstrate the significant effects of filter membrane choice.

3.1.5. *Light scattering contributions from dispersed and aggregated LBG*

In previously reported SLS measurements on LBG solutions prepared using the 1200-SFCA protocol (O'Connell et al., 2023); we observed power law static scattering profiles characterised by exponents of ~ -2.8 across the entire measured concentration range (0.006–0.83 wt%); we assigned this behaviour to aggregates that dominate the scattering and mask the dispersed polymer contribution. AF4 naturally allows these two contributions to be separated and observed individually: the scattering profile for each fraction may be determined by integration of the MALS signals over the relevant elution time window. The result of this procedure is shown in Fig. 9.

The dispersed polymer contribution is highly consistent across the three protocols: a plateau is observed at low q and the data are well

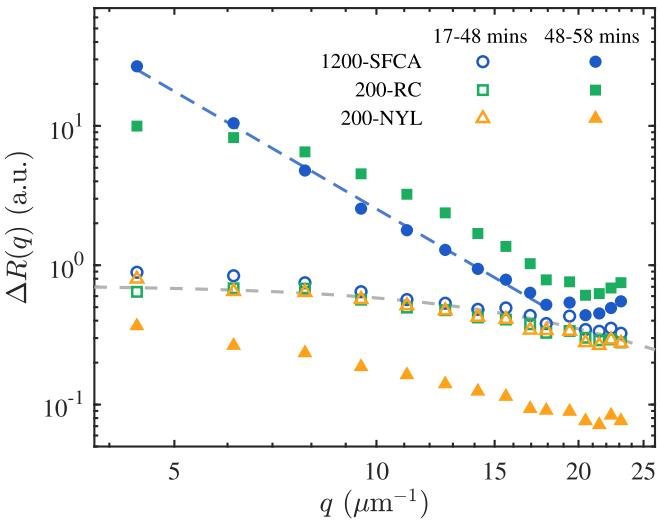

Fig. 9. AF4-MALS profiles for LBG solutions following each of the three filtration treatments. The MALS data have been integrated over the dispersed polymer (17–48 min, open symbols) and aggregated (48–58 min, closed symbols) regions. The blue dashed line marks a slope of −2.8, while the grey dashed line shows the Debye scattering function (Eq. 2) with $R_g = 82.1$ nm.

described by the Debye scattering function (Eq. 2) across the probed scattering vector (q) range, with R_g set to the intensity-averaged value determined earlier from integration of the 200-NYL data (82.1 nm). For the 1200-SFCA sample, the aggregate contribution clearly dominates that of the dispersed polymer, showing a power law profile with slope of ~ -2.8, fully consistent with our previous bulk SLS measurements (O'Connell et al., 2023). For the 200-RC sample, the aggregate scattering is still dominant, though the data approach a plateau towards low q, reflecting the reduced maximum aggregate radius. The 200-NYL sample, in contrast, shows significantly weaker scattering in the aggregate elution window, consistent with the removal of most of the aggregates; the data may contain contributions from a small fraction of remaining aggregates as well as from the largest dispersed LBG molecules. Notably, following this protocol, the aggregate contribution is sufficiently low that the dispersed polymer scattering dominates.

This analysis confirms our previous hypothesis—that the dispersed polymer scattering from unfractionated 1200-SFCA samples (characterised by SLS, not AF4-MALS) was largely obscured by the aggregates—as well as suggesting that the 200-NYL protocol provides a means to prepare samples where this is not the case. To further investigate this, samples were prepared at several concentrations following the 200-NYL protocol, and characterised using SLS and DLS; these results are presented in the following section.

3.2. Concentration-dependent SLS and DLS on LBG solutions prepared using the 200-NYL protocol

SLS and DLS measurements were performed on solutions prepared using the 200-NYL protocol at six concentrations ranging from 0.018 to 1.1 wt%. The excess Rayleigh ratio is shown as a function of scattering wavevector (q) in Fig. 10. As discussed above, similar experiments for 1200-SFCA samples demonstrated SLS data characterised by power law

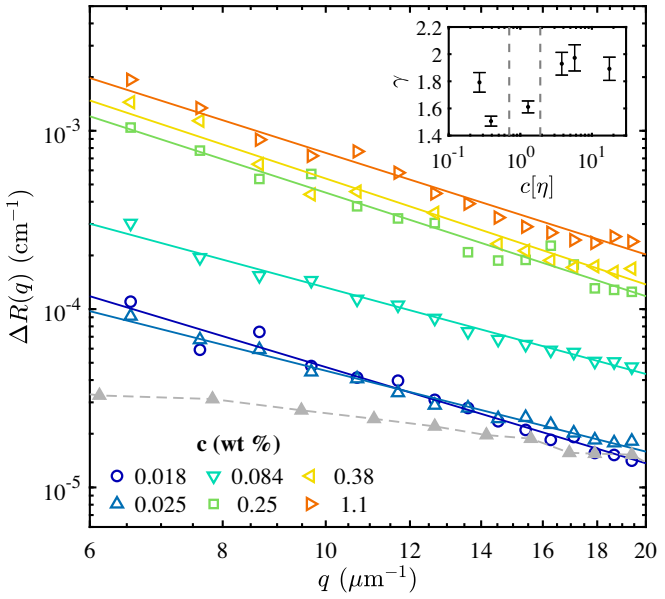

Fig. 10. Excess Rayleigh ratio, $\Delta R(q)$, against scattering wavevector, q, for LBG solutions prepared following the 200-NYL protocol. Solid lines are linear fits, and the inset shows the negative of the fitted slopes, γ, against reduced concentration, $c[\eta]$. Grey dashed lines in the inset demarcate the viscosity regimes previously identified from steady shear rheology of 1200-SFCA solutions: dilute (left), semidilute unentangled (center), semidilute entangled (right) (O'Connell et al., 2023). In the main plot, the grey filled triangles connected by a dashed line denote the total scattering from 200-NYL as measured by AF4-MALS (integrated over elution times 17–58 min, covering both the dispersed and aggregated fractions), rescaled to overlay the lowest concentration SLS results at high q.

scattering, with the excess Rayleigh ratio following $\sim q^{-2.8}$, attributed to the dominant scattering profile for the aggregated LBG fraction (O'Connell et al., 2023). It was expected that the strict nylon filtration of the 200-NYL protocol (which reduced the aggregate scattering observed in AF4 to a non-dominant level) would lead to scattering plateaus at low q, especially for dilute solutions, where the dispersed polymer would primarily be observed. However, the scattering profiles exhibit power law decays across the range of q and concentrations probed, with no indication of low q plateaus.

As the AF4 results showed a small remaining aggregate fraction following the 200-NYL protocol (see Fig. 6), this seems a likely origin of the excess scattering at low q. To investigate this and provide a direct comparison between the AF4 and bulk SLS data, the AF4-MALS signals for 200-NYL were integrated over both the dispersed and the aggregated fraction (17–58 min, i.e. the sum of the two components shown in Fig. 9). These data are shown in Fig. 10 (solid grey triangles), with an arbitrary scaling applied to overlap the high-q region of the bulk SLS data for the most dilute solution. Notably, the combined AF4-MALS contributions still show a clear low q plateau, which the bulk SLS data strongly diverge from, indicating that the unfractionated sample scattering is not simply the sum of the two fractions observed by AF4. This suggests that unfractionated samples undergo further 'secondary' aggregation after filtration, either forming aggregates which are weak enough to be broken by the AF4 flow conditions, or occurring over a longer timescale (as described in Section 2.2, samples for concentration-dependent SLS and DLS were prepared by concentration or dilution of the filtered 200-NYL stock, and were left overnight before measurement; in contrast, AF4 measurements were made shortly after filtration); our previous results suggested the presence of secondary aggregation occurring in 1200-SFCA samples following filtration (O'Connell et al., 2023). While the excess scattering at low q persists and the scattering profiles still show power law behaviour, the 200-NYL scattering intensities are overall greatly reduced compared to our previously reported 1200-SFCA results, reflecting the significant removal of material upon the additional filtration (O'Connell et al., 2023).

The scattering profiles were fitted with power laws of the form $\Delta R(q) = Aq^{-\gamma}$, and the magnitudes of the fitted slopes (γ) are shown in the inset of Fig. 10. The slopes are in the range 1.5–2.0, notably lower than the range of 2.7–3.1 found for 1200-SFCA samples (O'Connell et al., 2023). This range roughly agrees with the expectations for neutral flexible linear polymers (from 1.7 for good solvent conditions to 2.0 for θ conditions), suggesting that the aggregates here are much looser in structure than those of the 1200-SFCA samples. Note that we compare the power law slopes to those expected for neutral linear polymer at high q, where a plateau regime would be expected for $q < 1/R_g$. The slopes additionally indicate a slight concentration-dependence: for concentrations $\leq$ 0.084 wt%, γ lies in the range 1.5 to 1.8, while it is consistently ~ 2.0 for higher concentrations ($\geq$ 0.25 wt%). This is consistent with a conformation transition from extended coils to ideal random walks, as expected for flexible linear polymers upon screening of the excluded volume interaction within the semidilute regime. The transition is not clearly defined, though it appears to occur at a concentration between $c[\eta] = 1.3$ and $c[\eta] = 3.9$, roughly agreeing with the entanglement concentration previously determined for 1200-SFCA samples ($c^e[\eta] = 2.0 \pm 0.3$). Thus, while the unfractionated 200-NYL samples still appear to contain a fraction of aggregates (causing excess scattering at low q), these appear to be very loose, with their internal structure closely following the q-scaling and concentration-dependence expected for well-dispersed flexible linear polymers. Considering that the residual protein was shown to be removed by the 200-NYL protocol, we highlight that these results directly show supramolecular aggregation occurring between LBG molecules in the absence of protein.

Considering DLS, our previously reported results for 1200-SFCA samples showed a single stretched exponential 'slow' decay mode for $c < c^e$, and an additional 'fast' mode appearing in the semi-dilute

concentration range for $c > c^e$ (O'Connell et al., 2023). The slow mode decay rate scaled with q^3 and was attributed to internal relaxations within supramolecular aggregates, while the fast mode scaled with q^2, was concentration-independent (where present), and was assigned to cooperative diffusion (Burchard & Richtering, 1989; O'Connell et al., 2023). The results for the 200-NYL samples are discussed briefly here, and presented in more depth in the SI (Appx. E). Overall, the same behaviour was observed, with the intensity autocorrelation functions (Fig. S2 (SI)) again showing a slow mode which scales with q^3 at all concentrations, and a diffusive fast mode appearing for $c > c^e$. The data were fitted following the approach previously developed: a single stretched exponential for $c \leq 0.084$ wt% and double stretched exponentials for $c \geq 0.25$ wt% (O'Connell et al., 2023), allowing for extraction of decay amplitudes, timescales, and stretching parameters. The slow mode timescales could be fitted to determine an apparent local specific viscosity, using a relation derived from the Zimm model (Adam & Delsanti, 1977; Doi & Edwards, 1986; O'Connell et al., 2023); this is shown in Fig. S7 (SI), overlaid with bulk specific viscosity data previously found for 1200-SFCA samples O'Connell et al. (2023). As found previously, the data roughly overlap within the semidilute range, although a larger value of the Zimm scaling constant was required here to make the two datasets comparable (1.3, c.f. 0.45 used for the solutions without nylon filtration) (O'Connell et al., 2023).

The most significant difference between the results for the two protocols is in the amplitudes of the two modes (Fig. S3 (SI)) where present: the fast mode amplitude for the 200-NYL samples is generally around three times larger than that observed for the 1200-SFCA samples, reflecting its association with the dispersed polymer fraction which becomes comparatively more significant upon the removal of the aggregates. Despite this, the fast mode timescale (Fig. S5 (SI)) is almost consistent with that observed in the 1200-SFCA samples (with a diffusion coefficient of $\langle D_f \rangle_c = 4.8 \pm 0.1$ $\mu m^2 s^{-1}$, c.f. $\langle D_f \rangle_c = 5.8 \pm 0.3$ $\mu m^2 s^{-1}$ found previously), showing that the 200-NYL protocol has minimal impact on the dispersed polymer fraction itself.

In summary, the 200 nm nylon membrane filtration reduces the aggregated LBG fraction sufficiently to allow the dispersed polymer scattering to be probed. The static scattering profiles follow power law decays; remaining excess scattering at low q indicates persistent weak aggregation, while the smaller absolute values of the scattering slopes suggest internal structures consistent with the expectation for well-dispersed linear polymers. The fast mode in DLS—associated with the dispersed LBG—becomes relatively greater in amplitude owing to the reduction of the aggregate fraction and its associated slow mode, while the q-dependence and timescales of the fast mode are largely unaffected, reflecting the negligible effect on the dispersed fraction as indicated by the AF4 results.

3.3. Effect of solvent conditions

Ionic strength and pH are known to impact polymer solution properties such as solubility, conformation, rheology, and associative behaviour, often with particularly strong effects on polyelectrolytes (including proteins) (Dai et al., 2001; Doyle et al., 2009; Morris et al., 1980; Rinaudo et al., 1993; Xiong, 1992). For LBG, it has previously been suggested that a phosphate buffer at pH 8 may reduce associations between galactose-poor backbone regions, inhibiting aggregation (Richardson et al., 1998; Sébastien et al., 2014). To investigate this, and any effect of increased ionic strength during solubilisation, LBG samples were prepared in modified solvent conditions, following protocols NITR (0.1 M sodium nitrate ($NaNO_3$)) and PHOS (50 mM phosphate buffer solution (pH = 8)), as described in Section 2.2, and characterised by AF4. For the NITR and PHOS protocols, the carrier fluid used for AF4 measurement matched the solvent used in preparation. 1200-SFCA results are used for comparison throughout this section; here, water was used as the solvent for sample preparation, while the carrier fluid used for AF4 was that of the NITR protocol.

The AF4 elution profiles (signals from the RI detector, MALS at 90 and 20°, and UV absorption at 280 nm) are shown in Fig. S9 (SI) for samples following both the NITR and PHOS protocols, alongside the 1200-SFCA data for comparison; R_g and M determined throughout elution are shown in Fig. S10 (SI), with repeat data in Fig. S8 (SI). The resulting conformation plot (constructed as in Section 3.1.4) is shown in Fig. 11.

For the NITR protocol, the data are generally consistent with those of the 1200-SFCA sample; the dispersed polymer fraction displays very similar behaviour and the aggregated fraction also shows good overlap, particularly towards the higher molecular weight range. The data for the dispersed fraction were fitted with a power law, as in Section 3.1.4, and the Flory exponent was estimated as $\nu = 0.64 \pm 0.01$, consistent with the value determined for 1200-SFCA (0.63 ± 0.01); as before, we stress that the exponent is based on data spanning less than an order of magnitude and should thus be treated with caution; however, it is clear that the behaviour is very similar between the two protocols. Recalling that the carrier fluid used for AF4 characterisation of the 1200-SFCA samples was the solvent used in the preparation and characterisation of the NITR samples, the consistency between the results might not be surprising; however, the results do confirm that there are no significant effects of increased ionic strength during solubilisation.

For the PHOS protocol, the dispersed fraction is again generally consistent, and was described by a power law with Flory exponent of $\nu = 0.63 \pm 0.01$, consistent with the values found for all other protocols. Notably, the aggregate fraction is still present, showing that preparation in the phosphate buffer did not significantly inhibit aggregate formation as has previously been suggested (Richardson et al., 1998; Sébastien et al., 2014). However, the aggregates are lower in molecular weight ($\approx 5 \times 10^7 - 2 \times 10^9$ g mol^{-1}, compared to $2 \times 10^8 - 3 \times 10^{10}$ g mol^{-1} observed for 1200-SFCA) and also somewhat lower in size, suggesting reduced intermolecular interactions in the phosphate buffer. This could be due both to a reduction in LBG-LBG association, or, recalling that the aggregates contain residual protein, to changes in the LBG-protein or protein-protein interactions. An effect involving proteins seems plausible considering that protein surface charges will be modified by the increased buffer pH (Guseman et al., 2018; Yang & Honig, 1993). In

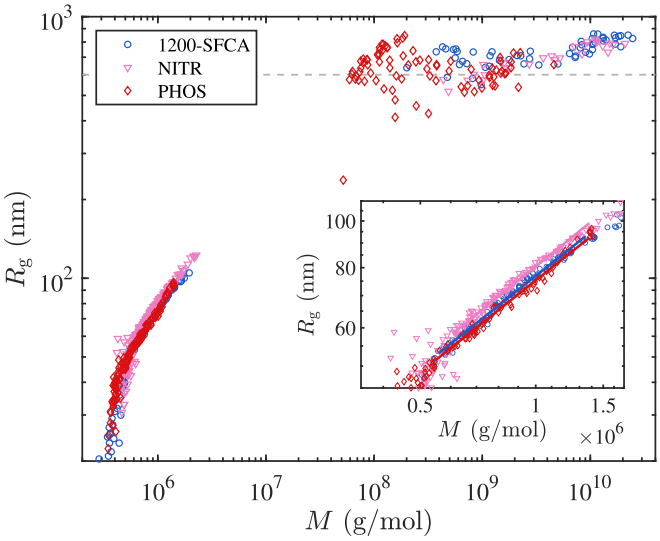

Fig. 11. Conformation plot of R_g versus M, based on AF4-MALS data. The dashed line marks the filtration radius used in sample preparation (600 nm). The inset shows an expanded view of the fitted region; solid lines are linear fits to the data they span, with slopes of $\nu = 0.63 \pm 0.01$ for the 1200-SFCA protocol, $\nu = 0.64 \pm 0.01$ for the NITR protocol, and $\nu = 0.63 \pm 0.01$ for the PHOS protocol.

contrast, galactomannans are expected to remain neutral across a wide pH range, undergoing deprotonation and adopting an ionic nature only in highly alkaline conditions, as has been observed for LBG and fenugreek gums at pH ~ 12 or higher (this transition may be understood in relation to the pK_a values of the constituent sugar residues: 12.1 and 12.4 for mannose and galactose, respectively) (Doyle et al., 2009; Goycoolea et al., 1995; Rovio et al., 2007).

4. Conclusion

Asymmetric flow field-flow fractionation was used to characterise the structure of locust bean gum in solution. The dispersed and aggregated polymer fractions were successfully separated and characterised with respect to molecular weight and size via coupling to multi-angle laser light scattering (MALS), refractive index (RI), and UV/VIS detectors.

The aggregate fraction was strongly dependent on the filtration used during preparation. Using a 1.2 μm SFCA filter, the aggregates had masses of $2 \times 10^8 - 3 \times 10^{10}$ g mol^{-1}, and radii of ~ 600–800 nm, and appeared to be formed by filter-induced breaking and compression of significantly larger aggregates, characteristic of the solutions prior to filtration. Following additional filtration with a 200 nm RC filter, aggregates were reduced in size and mass (to ~ 200 − 400 nm, $1 \times 10^8 - 4 \times 10^9$ g mol^{-1}), but were not removed, despite being much larger (~ 6–8 times) than the filtration pore size. In contrast, a 200 nm filter with a nylon membrane largely removed the aggregates, yet with minimal impact on the dispersed LBG distribution. Notably, a residual protein fraction was observed to co-elute with the aggregates (and was removed along with the aggregates by the nylon filtration), raising the possibility that protein is a key component of the aggregates, and suggesting a role of protein in aggregate formation.

In contrast, the well-dispersed LBG was relatively unaffected by the filtration procedure, being characterised by R_g of 40–100 nm and masses of $3 \times 10^5 - 1.5 \times 10^6$ g mol^{-1}, respectively, with the distribution approximately following Flory scaling ($R_g \sim M^\nu$) with exponent $\nu \sim 0.63$. The aggregate fraction, where present, skewed the R_g and M determined as a function of elution time before the full dispersed distribution could be observed (starting at ~ 80 % mass recovery, while the final mass recovery was 94 %). Following filtration with a nylon filter, the upper end of the distribution could be observed without interference from the aggregate elution. For this protocol, size and mass distribution averages (weighted by number, mass, and intensity) were determined as: $R_{g,n} = 66.0$ nm, $R_{g,w} = 74.9$ nm, $R_{g,z} = 82.1$ nm, $M_n = 7.5 \times 10^5$ g mol^{-1}, $M_w = 9.2 \times 10^5$ g mol^{-1}, and $M_z = 1.1 \times 10^6$ g mol^{-1}, with a dispersity of 1.22.

By separating the dispersed and aggregated fractions, we confirmed that light scattering on aqueous LBG solutions, prepared using 1.2 μm SFCA membrane filtration, was dominated by the aggregate contribution. We also demonstrated that an additional 200 nm nylon filtration effectively removed the aggregates, such that the dispersed polymer scattering dominated. However, we observed an excess in static light scattering (SLS) when compared to the AF4-MALS data integrated over the full elution, demonstrating residual weak aggregation in unfractionated samples even at dilute concentrations (arising from LBG association in the absence of protein). The SLS profiles were well described by power laws ($\Delta R(q) \sim q^{-\gamma}$), where $\gamma \sim 1.5$–2.0, demonstrating scattering from within significantly 'looser' aggregates when compared to those observed without the additional filtration (characterised by $\gamma \sim 2.8$ and significantly higher scattering intensities).

DLS measurements on the additionally filtered samples showed a slow decay mode characterised by q^3-dependent characteristic decay rates, consistent with Zimm behaviour, as expected for scattering from structures within aggregates (O'Connell et al., 2023). A secondary fast mode, assigned to cooperative diffusion mainly within the dispersed fraction, was observed within the semi-dilute concentration range. Compared to previous measurements on LBG solutions prepared without additional filtration (O'Connell et al., 2023), the slow mode amplitude was much weaker, due to the reduced remaining aggregate fraction, while the timescale of the fast mode was unchanged, further demonstrating the low impact of the additional filtration on the dispersed polymer fraction.

Finally, we demonstrated the impact of solution pH and ionic strength on both the dispersed and aggregate fractions. The solution structure was shown to be relatively unaffected by increased ionic strength (0.1 M $NaNO_3$), while a pH 8 phosphate buffer led to smaller aggregates of lower mass ($\approx 5 \times 10^7 - 2 \times 10^9$ g mol^{-1}), indicating a reduction in intermolecular association, without largely impacting the dispersed fraction.

In summary, AF4 proved to be powerful in characterising aqueous solutions of LBG—an industrially significant high molecular weight polymer with a strong tendency to aggregate even in dilute solutions. Using AF4, we were able to provide a detailed characterisation of both the dispersed and aggregate fractions of these solutions. Furthermore, the AF4 method allowed investigation of how changes to solution conditions, such as pH and ionic strength, affect both fractions. We expect this powerful method to be similarly applicable to other galactomannans, and indeed other high molecular weight and/or associating polymers, making it a highly valuable tool for polymer characterisation both within industry and academia.

CRediT authorship contribution statement

Adam O'Connell: Conceptualization, Investigation, Data curation, Formal analysis, Visualization, Methodology, Writing - original draft, Writing - review & editing. **Yadira González-Espinosa:** Methodology, Investigation, Validation, Data curation, Formal analysis, Writing – review & editing. **Francisco M. Goycoolea:** Methodology, Resources, Writing – review & editing, Supervision, Funding acquisition. **Peter Schuetz:** Resources, Writing – review & editing, Supervision, Funding acquisition. **Johan Mattsson:** Conceptualization, Resources, Supervision, Funding acquisition, Methodology, Writing - review & editing.

Declaration of competing interest

The authors declare that they have no known competing financial interests or personal relationships that could have appeared to influence the work reported in this paper.

Data availability

The data in this paper are available in the Leeds Data Repository (https://doi.org/10.5518/1353).

Acknowledgements

The authors acknowledge financial support from the Engineering and Physical Sciences Research Council (EPSRC) funded Centre for Doctoral Training in Soft Matter and Functional Interfaces (grant EP/L015536/1). We acknowledge financial support from the School of Food Science and Nutrition, University of Leeds, to enable the AF4 studies. We also thank the EPSRC for funding the photon correlation spectrometer used in the work on grant EP/J021156/1. J. M. is grateful for support from EPSRC on grant EP/K005073/1. We thank Paul Clarke and Bassem Sabagh (Postnova, UK) for technical support and review of the manuscript.

Appendix A. Supplementary data

Supplementary data to this article can be found online at https://doi.org/10.1016/j.carbpol.2023.121286.

References

Adam, M., & Delsanti, M. (1977). Dynamical properties of polymer solutions in good solvent by Rayleigh scattering experiments. *Macromolecules, 10*, 1229–1237. https://doi.org/10.1021/ma60060a014

Andersson, M., Wittgren, B., & Wahlund, K. G. (2003). Accuracy in multiangle light scattering measurements for molar mass and radius estimations. Model calculations and experiments. *Analytical Chemistry, 75*, 4279–4291. https://doi.org/10.1021/ac030128+

Armistead, S. J., Smith, C. C., & Staniland, S. S. (2022). Sustainable biopolymer soil stabilization in saline rich, arid conditions: A 'micro to macro' approach. *Scientific Reports, 12*, 1–11. https://doi.org/10.1038/s41598-022-06374-6

Barak, S., & Mudgil, D. (2014). Locust bean gum: Processing, properties and food applications—A review. *International Journal of Biological Macromolecules, 66*, 74–80. https://doi.org/10.1016/j.ijbiomac.2014.02.017

Berry, G. C., & Cotts, P. M. (1999). Static and dynamic light scattering. In R. A. Pethrick, & J. V. Dawkins (Eds.), *Modern techniques for polymer characterisation* (pp. 81–108). London: John Wiley & Sons, Ltd.

Biliaderis, C. G., & Izydorczyk, M. S. (2006). Functional food carbohydrates. *CRC Press.*. https://doi.org/10.1201/9781420003512

Borsali, R., & Pecora, R. (2008). *Soft matter characterization*. New York: Springer.

Burchard, W., & Richtering, W. (1989). Dynamic light scattering from polymer solutions. In M. Pietralla, & W. Pechhold (Eds.), *Relaxation in polymers* (pp. 151–163). Darmstadt: Steinkopff.

Cerqueira, M. A., Bourbon, A. I., Pinheiro, A. C., Martins, J. T., Souza, B. W. S., Teixeira, J. A., & Vicente, A. A. (2011). Galactomannans use in the development of edible films/coatings for food applications. *Trends in Food Science & Technology, 22*, 662–671. https://doi.org/10.1016/j.tifs.2011.07.002

Cochereau, R., Nicolai, T., Chassenieux, C., & Silva, J. V. (2019). Mechanism of the spontaneous formation of plant protein microcapsules in aqueous solution. *Colloids and Surfaces A: Physicochemical and Engineering Aspects, 562*, 213–219. https://doi.org/10.1016/j.colsurfa.2018.11.019

Colby, R. H. (2010). Structure and linear viscoelasticity of flexible polymer solutions: Comparison of polyelectrolyte and neutral polymer solutions. *Rheologica Acta, 49*, 425–442. https://doi.org/10.1007/s00397-009-0413-5

Cölfen, H., & Antonietti, M. (2000). Field-flow fractionation techniques for polymer and colloid analysis. In M. Schmidt (Ed.), *New developments in polymer analytics I* (pp. 67–187). Berlin Heidelberg, Berlin, Heidelberg: Springer. https://doi.org/10.1007/3-540-48764-6_2.

Coppen, J. J. W., & Food and Agriculture Organization of the United Nations. (1995). *Gums, resins and latexes of plant origin*. Food and Agriculture Organization of the United Nations.

Dai, S., Tam, K. C., & Jenkins, R. D. (2001). Light scattering of hydrophobically modified alkali-soluble emulsion (hase) polymer: Ionic strength and temperature effects. *Macromolecular Chemistry and Physics, 202*, 335–342. https://doi.org/10.1002/1521-3935(20010101)202:2<335::AID-MACP335>3.0.CO;2-H

Debye, P. (1947). Molecular-weight determination by light scattering. *The Journal of Physical and Colloid Chemistry, 51*, 18–32. https://doi.org/10.1021/j150451a002

Doi, M., & Edwards, S. F. (1986). *The theory of polymer dynamics*. Oxford: Oxford University Press.

Doublier, J. L., & Launary, B. (1981). Rheology of galactomannan solutions: Comparative study of guar gum and locust bean gum. *Journal of Texture Studies, 12*, 151–172.

Doyle, J. P., Lyons, G., & Morris, E. R. (2009). New proposals on "hyperentanglement" of galactomannans: Solution viscosity of fenugreek gum under neutral and alkaline conditions. *Food Hydrocolloids, 23*, 1501–1510. https://doi.org/10.1016/j.foodhyd.2008.09.007

Dumitriu, S. (2004). *Polysaccharides*. Marcel Dekker.

Edelhoch, H. (1967). Spectroscopic determination of tryptophan and tyrosine in proteins. *Biochemistry, 6*, 1948–1954. https://doi.org/10.1021/bi00859a010

Ellison, A. J., Senaratne, W., & Wei, Y. (2008). *Gum coatings for cell culture, methods of manufacture and methods of use*.

Gaisford, S. E., Harding, S. E., Mitchell, J. R., & Bradley, T. D. (1986). A comparison between the hot and cold water soluble fractions of two locust bean gum samples. *Carbohydrate Polymers, 6*, 423–442. https://doi.org/10.1016/0144-8617(86)90002-0

de Gennes, P. G. (1979). *Scaling concepts in polymer physics*. London: Cornell University Press.

Gentile, L. (2020). Protein–polysaccharide interactions and aggregates in food formulations. *Current Opinion in Colloid and Interface Science, 48*, 18–27. https://doi.org/10.1016/j.cocis.2020.03.002

González-Espinosa, Y., Sabagh, B., Moldenhauer, E., Clarke, P., & Goycoolea, F. M. (2019). Characterisation of chitosan molecular weight distribution by multi-detection asymmetric flow-field flow fractionation (AF4) and SEC. *International Journal of Biological Macromolecules, 136*, 911–919. https://doi.org/10.1016/j.ijbiomac.2019.06.122

Goycoolea, F. M., Morris, E. R., & Gidley, M. J. (1995). Viscosity of galactomannans at alkaline and neutral pH: Evidence of 'hyperentanglement' in solution. *Carbohydrate Polymers, 27*, 69–71. https://doi.org/10.1016/0144-8617(95)00030-B

Grenha, A., & Dionísio, M. (2012). Locust bean gum: Exploring its potential for biopharmaceutical applications. *Journal of Pharmacy & Bioallied Sciences, 4*, 175. https://doi.org/10.4103/0975-7406.99013

Guseman, A. J., Speer, S. L., Perez Goncalves, G. M., & Pielak, G. J. (2018). Surface charge modulates protein–protein interactions in physiologically relevant environments. *Biochemistry, 57*, 1681–1684.

Joshi, V., & Chernokalskaya, E. (2011). Filtration as a sample preparation technique prior to mass spectrometry: Selecting the right filtration device. *Sample Preparation in Biological Mass Spectrometry, 61–75*. https://doi.org/10.1007/978-94-007-0828-0_4

Kawamura, Y. (2016). Carob bean gum, 82nd JECFA—Chemical and technical assessment (CTA). In *Technical Report* (pp. 1–10). Rome: FAO.

Kim, Y. B., Yang, J. S., & Moon, M. H. (2018). Investigation of steric transition with field programming in frit inlet asymmetrical flow field-flow fractionation. *Journal of Chromatography A, 1576*, 131–136. https://doi.org/10.1016/j.chroma.2018.09.036

Kowalkowski, T., Sugajski, M., & Buszewski, B. (2018). Impact of ionic strength of carrier liquid on recovery in flow field-flow fractionation. *Chromatographia, 81*, 1213–1218. https://doi.org/10.1007/s10337-018-3551-z

Liu, X., Shen, L., Zhao, S., Zhang, H., 2021. Formation and emulsification properties of self-assembled potato protein microgel particles under different ph conditions. International Journal of Food Science & Technology 56, 2864–2875. doi: https://doi.org/10.1111/ijfs.14923, arXiv: https://ifst.onlinelibrary.wiley.com/doi/pdf/10.1111/ijfs.14923.

Lopes da Silva, J. A., & Goncalves, M. P. (1990). Studies on a purification method for locust bean gum by precipitation with isopropanol. *Food Hydrocolloids, 4*, 277–287. https://doi.org/10.1016/S0268-005X(09)80204-X

Makan, A. C., Otte, T., & Pasch, H. (2012). Analysis of high molar mass branched polybutadienes by SEC-MALLS and AF4-MALLS. *Macromolecules, 45*, 5247–5259. https://doi.org/10.1021/ma3007812

Martin, J. E., & Hurd, A. J. (1987). Scattering from fractals. *Journal of Applied Crystallography, 20*, 61–78. https://doi.org/10.1107/S0021889887087107

McCleary, B. V., & Matheson, N. K. (1974). A-D-galactosidase activity and galactomannan and galactosylsucrose oligosaccharide depletion in germinating legume seeds. *Phytochemistry, 13*, 1747–1757.

McCleary, B. V., & Matheson, N. K. (1975). Galactomannan structure and β-mannanase and β-mannosidase activity in germinating legume seeds. *Phytochemistry, 14*, 1187–1194. https://doi.org/10.1016/S0031-9422(00)98592-3

McClements, D. J. (2006). Non-covalent interactions between proteins and polysaccharides. *Biotechnology Advances, 24*, 621–625. https://doi.org/10.1016/j.biotechadv.2006.07.003

Morris, E. R., Rees, D. A., & Welsh, E. (1980). Conformation and dynamic interactions in hyaluronate solutions. *Journal of Molecular Biology, 138*, 383–400. https://doi.org/10.1016/0022-2836(80)90294-6

Myers, M. N., & Giddings, J. C. (1982). Properties of the transition from Normal to steric field-flow fractionation. *Analytical Chemistry, 54*, 2284–2289. https://doi.org/10.1021/ac00250a032

Newburger, S. H. (1961). Industrial gums: Polysaccharides and their derivatives. *Journal of AOAC International, 44*, 804. https://doi.org/10.1093/jaoac/44.4.804a

O'Connell, A., Goycoolea, F. M., Gulotta, A., Holmqvist, P., Schuetz, P., & Mattsson, J. (2023). The structure and dynamics of locust bean gum in aqueous solution. *Food Hydrocolloids, 138*, Article 108446. https://doi.org/10.1016/j.foodhyd.2022.108446

Otte, T., Pasch, H., Macko, T., Brüll, R., Stadler, F., Kaschta, J., Becker, F., & Buback, M. (2011). Characterization of branched ultrahigh molar mass polymers by asymmetrical flow field-flow fractionation and size exclusion chromatography. *Journal of Chromatography A, 1218*, 4257–4267. https://doi.org/10.1016/j.chroma.2010.12.072

Perestrelo, A. R., Grenha, A., Rosa Da Costa, A. M., & António Belo, J. (2014). Locust bean gum as an alternative polymeric coating for embryonic stem cell culture. *Materials Science and Engineering: C, 40*, 336–344. https://doi.org/10.1016/j.msec.2014.04.022

Picout, D. R., & Ross-Murphy, S. B. (2007). On the mark–Houwink parameters for galactomannans. *Carbohydrate Polymers, 70*, 145–148.

Picout, D. R., Ross-Murphy, S. B., Errington, N., & Harding, S. E. (2001). Pressure cell assisted solution characterization of polysaccharides. 1. *Guar gum. Biomacromolecules, 2*, 1301–1309. https://doi.org/10.1021/bm010118n

Picout, D. R., Ross-Murphy, S. B., Jumel, K., & Harding, S. E. (2002). Pressure cell assisted solution characterization of polysaccharides. 2. Locust bean gum and tara gum. *Biomacromolecules, 3*, 761–767. https://doi.org/10.1021/bm025517c

Prajapati, V. D., Jani, G. K., Moradiya, N. G., Randeria, N. P., Nagar, B. J., Naikwadi, N. N., & Variya, B. C. (2013). *Galactomannan: A versatile biodegradable seed polysaccharide*. https://doi.org/10.1016/j.ijbiomac.2013.05.017. arXiv:0005074v1.

Richardson, P. H., Willmer, J., & Foster, T. J. (1998). Dilute solution properties of guar and locust bean gum in sucrose solutions. *Food Hydrocolloids, 12*.

Richter, S., Boyko, V., Matzker, R., & Schröter, K. (2004). Gelation studies: Comparison of the critical exponents obtained by dynamic light scattering and rheology, 2a. A thermoreversible gelling system: Mixtures of xanthan gum and locust-bean gum. *Macromolecular Rapid Communications, 25*, 1504–1509. https://doi.org/10.1002/marc.200400214

Rinaudo, M., Milas, M., & Le Dung, P. (1993). Characterization of chitosan. Influence of ionic strength and degree of acetylation on chain expansion. *International Journal of Biological Macromolecules, 15*, 281–285.

Rovio, S., Yli-Kauhaluoma, J., & Sirén, H. (2007). Determination of neutral carbohydrates by CZE with direct UV detection. *Electrophoresis, 28*, 3129–3135. https://doi.org/10.1002/elps.200600783

Rubinstein, M., & Colby, R. H. (2003). *Polymer physics*. Oxford: Oxford University Press.

Saha, D., & Bhattacharya, S. (2010). Hydrocolloids as thickening and gelling agents in food: A critical review. *Journal of Food Science and Technology, 47*, 587–597. https://doi.org/10.1007/s13197-010-0162-6. arXiv:arXiv:1011.1669v3.

Schärtl, W. (2007). *Light scattering from polymer solutions and nanoparticle dispersions*. Berlin Heidelberg: Springer.

Schätzel, K. (1987). Correlation techniques in dynamic light scattering. *Applied Physics B Photophysics and Laser Chemistry, 42*, 193–213. https://doi.org/10.1007/BF00693937

Schmid, F. X. (2001). Biological macromolecules: UV-visible spectrophotometry. *Encyclopedia of Life Sciences, 1–4*. https://doi.org/10.1038/npg.els.0003142

Sébastien, G., Christophe, B., Mario, A., Pascal, L., Michel, P., & Aurore, R. (2014). Impact of purification and fractionation process on the chemical structure and physical properties of locust bean gum. *Carbohydrate Polymers, 108*, 159–168. https://doi.org/10.1016/j.carbpol.2014.02.092

Sutton, R. L., Cooke, D., & Russell, A. (1997). Recrystallization in sugar/stabilizer solutions as affected by molecular structure. *Journal of Food Science, 62*, 1145–1149. https://doi.org/10.1111/j.1365-2621.1997.tb12232.x

Tagad, C. K., Rajdeo, K. S., Kulkarni, A., More, P., Aiyer, R. C., & Sabharwal, S. (2014). Green synthesis of polysaccharide stabilized gold nanoparticles: Chemo catalytic and room temperature operable vapor sensing application. *RSC Advances, 4*, 24014–24019. https://doi.org/10.1039/c4ra02972k

Ventura, M. G., Paninho, A. I., Nunes, A. V., Fonseca, I. M., & Branco, L. C. (2015). Biocompatible locust bean gum mesoporous matrices prepared by ionic liquids and a scCO2 sustainable system. *RSC Advances, 5*, 107700–107706. https://doi.org/10.1039/c5ra17314k

Woo, S., Lee, J. Y., Choi, W., & Moon, M. H. (2016). Characterization of ultrahigh-molecular weight cationic polyacrylamide using frit-inlet asymmetrical flow field-flow fractionation and multi-angle light scattering. *Journal of Chromatography A, 1429*, 304–310. https://doi.org/10.1016/j.chroma.2015.12.027

Wu, H. (2010). Correlations between the Rayleigh ratio and the wavelength for toluene and benzene. *Chemical Physics, 367*, 44–47. https://doi.org/10.1016/j.chemphys.2009.10.019

Xiong, Y. L. (1992). Influence of ph and ionic environment on thermal aggregation of whey proteins. *Journal of Agricultural and Food Chemistry, 40*, 380–384.

Yang, A. S., & Honig, B. (1993). On the pH dependence of protein stability. *Journal of Molecular Biology, 231*, 459–474. https://doi.org/10.1006/jmbi.1993.1294

Young, R., & Lovell, P. (2011). *Introduction to polymers* (3 ed.). United States: CRC Press. https://doi.org/10.1201/9781439894156